




# Production of polylactic acid aerogels via phase separation and supercritical CO<sub>2</sub> drying: thermodynamic analysis of the gelation and drying process

Alberto Bueno<sup>1,\*</sup> , Christian Luebbert<sup>2</sup>, Sabine Enders<sup>3</sup>, Gabriele Sadowski<sup>2</sup>, and Irina Smirnova<sup>1</sup>

<sup>1</sup>Institute of Thermal Separation Processes, Hamburg University of Technology, Hamburg, Germany

<sup>2</sup>Laboratory of Thermodynamics, Department of Biochemical and Chemical Engineering, TU Dortmund University, Dortmund, Germany

<sup>3</sup>Institute of Technical Thermodynamics and Refrigeration Technology, KIT, Karlsruhe, Germany

Received: 6 April 2021

Accepted: 2 September 2021

© The Author(s) 2021

## ABSTRACT

The application range of aerogels, especially in the life-science sector, can be extended by utilizing biocompatible polymers such as polylactic acid (PLA). However, the low glass transition temperature ( $T_g$ ) of PLA and the challenging gelation techniques limit the application of supercritical CO<sub>2</sub> (scCO<sub>2</sub>) drying and thus the PLA-aerogel production. The aim of this work is to overcome this challenge and to provide a better understanding of the thermodynamics of the process. Therefore, the gelation of amorphous PLA (PDLLA) and semicrystalline PLA (PLLA) via thermal-induced phase separation (TIPS) was studied. To identify polymer/solvent/antisolvent ratios suitable for gelation, thermodynamic modeling (PC-SAFT) was used to describe the corresponding ternary phase diagrams. scCO<sub>2</sub> drying was used to preserve the mesoporous gel structure formed during the gelation. Due to the decrease in the  $T_g$  of PLA in the presence of CO<sub>2</sub>, this could not be applied to all gels. It was found that the critical parameter to enable the scCO<sub>2</sub> drying of low  $T_g$  polymers is the crystallinity degree ( $X_c$ ) of the polymer. Based on these results, some guidelines for producing aerogels from polymers with low  $T_g$  are formulated.

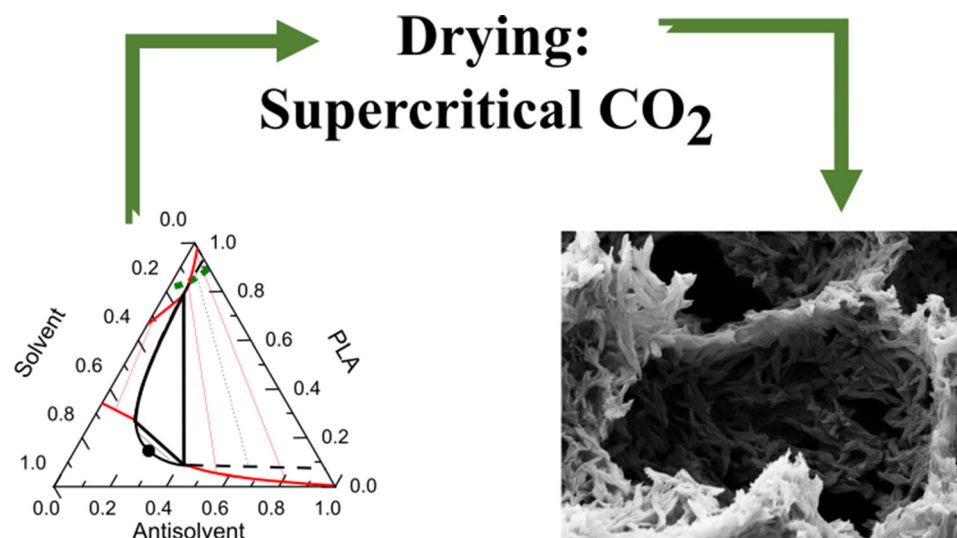
Handling Editor: Yaroslava Yingling.

Address correspondence to E-mail: alberto.bueno@tuhh.de

<https://doi.org/10.1007/s10853-021-06501-0>

Published online: 09 September 2021

## GRAPHICAL ABSTRACT



## Introduction

Most of the aerogels produced nowadays are produced from easily gelable starting materials such as silica via a sol-gel process [1], from alginate by crosslinking using divalent cations [2], from cellulose via a coagulation/gelation mechanism [3] or from synthetic polymers via various polymerization techniques [4]. The gels produced from these materials can be transformed readily to the corresponding aerogels by extracting the gelation solvent via a standard supercritical-drying process. The before-mentioned aerogels cover a wide range of applications such as thermal insulation, adsorption media, and active-compound carriers. But not all polymer-based gels are suitable for supercritical drying: Polymers with low  $T_g$  generally do not withstand the drying conditions losing their shape and porous structure. For instance, polylactic acid (PLA) could be effectively used as a drug carrier for pharmaceutical applications in the form of aerogels. However, until now, PLA-based aerogels exhibit still low surface areas, limiting their application's potential.

Polylactic acid (PLA) is a biocompatible, biodegradable and immunologically inert synthetic polymer, widely used in the pharmaceutical industry

as a carrier for active pharmaceutical ingredients (APIs). The chiral nature of lactic acid allows for preparing three types of PLA: PLLA (poly-L-lactic acid) and PDLA (poly-D-lactic acid) as well as PDLLA (poly-DL-lactic acid). The latter is a copolymer composed of both stereoisomers. PLLA is semicrystalline, while PDLA and PDLLA are both amorphous. In this paper, we use the term PLA for discussion of general mechanisms and processes for this type of polymers and specify later whenever appropriate if semicrystalline PLLA or amorphous PDLLA was used.

The possibility to transform raw PLA into a highly porous interconnected material (aerogel) increases the number of applications of PLA [5–9], e.g., in functional barriers (packaging), drug delivery, and tissue engineering. These applications would benefit from the opportunity to tailor the transport and adsorption of fluids in aerogels by adjusting the mesoporous and macroporous structure of the aerogel and thus, to achieve a large surface area and porosity. Depending on the final application, PLA aerogels can be generally produced in specific forms such as microparticles, membranes, or monoliths.

The mesoporous fraction of the porous structure can be determined via nitrogen adsorption, whereas a large BET surface area indicates the presence of

mesoporous fraction [10]. Salerno et al. report BET surface areas between 69 and 95  $\text{m}^2 \text{g}^{-1}$  using amorphous PDLLA and ethyl lactate [6]. Chen and Ma obtained BET surface areas of 91  $\text{m}^2 \text{g}^{-1}$  using semicrystalline PLLA and THF as the solvent [11]. Reverchon achieved surface areas of 45  $\text{m}^2 \text{g}^{-1}$  using semicrystalline PLLA with dioxane/ethanol as solvent/antisolvent system [12]. More recently, Rezabeigi et al. reported BET surface areas between 29 and 54  $\text{m}^2 \text{g}^{-1}$  for aerogels produced via phase separation [8] and between 45 and 61  $\text{m}^2 \text{g}^{-1}$  for corresponding foams produced by crystallization [13]. These surface areas are much lower than those of other organic aerogels (typically 200–500  $\text{m}^2 \text{g}^{-1}$ ), which could be explained by a low mesoporous fraction in the material. The question arises whether this pore structure formed this way during the gelation process or whether the mesoporous fraction was partly lost during the supercritical drying. Therefore, the aim of this work is to deeper understand the gelation and the drying processes, especially using the thermodynamic analysis of the corresponding systems.

For gel formation in polymeric systems, several techniques are known. The most widely used one is to exploit the phase separation of a polymer/solvent system. Decreasing the temperature (TIPS–thermal-induced phase separation) [11, 12, 14–19] and adding a non-solvent (NIPS–antisolvent-induced phase separation) are common triggers used to induce the phase separation of a solvent/polymer mixture, which will further develop into vitrified or crystallized porous structures [11, 14, 20, 21] and gel formation. The time between phase separation and the point when the mobility of the polymer-rich phase is reduced due to crystallization and/or crossing the glass transition is referred to as the gelation time.

van de Witte et al. [22–25] studied the phase diagrams of several solvent–antisolvent–PLLA and PDLLA systems relating the morphology of the obtained porous structures to different phase separation mechanisms. Other solvent systems such as dioxane/water, tetrahydrofuran, chloroform/methanol and dichloromethane/hexane have been used for NIPS of systems with semicrystalline PLLA and amorphous PDLLA [19, 24, 26].

To form an aerogel from a wet gel, it is necessary to remove the solvent without affecting the integrity of the porous structure. Depending on the mechanical toughness, the pore size of the gel structure, and

polymer–solvent interactions, different drying techniques can be applied. The most common drying methods used for drying PLA porous materials are evaporative drying and freeze-drying. In evaporative drying, the forces due to the surfaces tension of the vapor–liquid interface forming inside the pore may cause the porous structure to collapse [27]. To eliminate the surface tension during drying, most authors use freeze-drying [15, 16, 28]. Fewer authors use supercritical  $\text{CO}_2$  ( $\text{scCO}_2$ ) drying [6, 12]. As mentioned above, this technique is challenging to apply for PLA gels due to the low  $T_g$  of the PLA, which results in the gel collapse upon contact with  $\text{CO}_2$  during the supercritical drying process.

Thus, the goals of this work are twofold. The first goal is to improve the thermodynamic understanding of the gelation systems to identify suitable gelation conditions for aerogel production. The second aim is to overcome the difficulties during the  $\text{scCO}_2$  drying and establish guidelines to produce PLA-based aerogels by supercritical drying. Generally, the elaborated guidelines might be helpful for other polymers with low  $T_g$  as well.

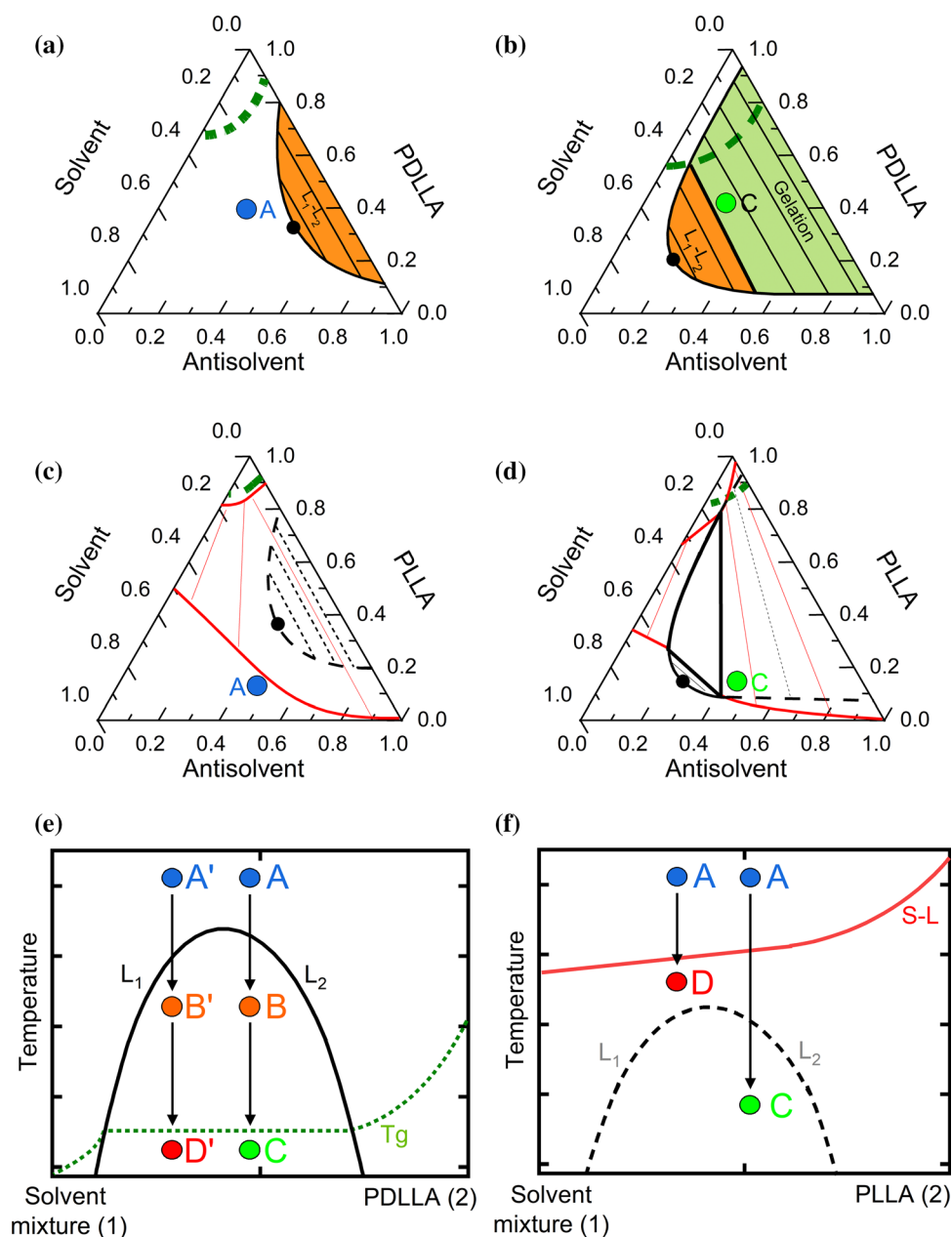
Consequently, the manuscript is divided into two main sections. The first section considers the gelation of semicrystalline and amorphous polymer–solvent systems using the TIPS technique and the representation of the system in pseudo-binary and ternary diagrams to understand the gelation process to identify suitable gelation areas. The experimental study is supported by phase-equilibrium modeling with PC-SAFT [29] and by  $T_g$  calculations [30]. The second section describes the effect of the drying procedure on the gels and suggests some general guidelines on how to perform the drying to obtain aerogels based on polymers having low  $T_g$ .

## Schematic phase diagrams

The gel formation mechanisms of the TIPS and NIPS processes can be best discussed using pseudo-binary and ternary phase diagrams (e.g., van de Witte et al. [22–25]). We combine and discuss here those diagram types, which is helpful to describe and to understand the phenomena occurring during our experimental procedures of gel formation.

Figure 1a–d shows ternary phase diagrams of typical polymer/solvent/antisolvent systems used for TIPS process at high temperatures (Fig. 1a, c) and

**Figure 1** Schematic phase diagrams of polymer/solvent/antisolvent mixtures. L-L demixing gaps are indicated by black lines, S-L phase separation lines are red. Thermodynamically stable phase separations are indicated as solid lines; metastable phase separations are indicated by dashed lines. Green dotted lines indicate the glass transition. Polymer does not crystallize in **a** and **b**, while it is semicrystalline in **c–f**. No gelation/demixing occurs for the mixture indicated by a blue symbol in **a**, gelation via LL-demixing occurs for the same composition at a lower temperature (**b**, green symbol). The gelation mechanism via crystallization is illustrated in **c** and **d**. The TIPS process is schematically depicted in **e** and **f**, which are pseudo-binary cuts for a given solvent/antisolvent mixture. Symbols in **e** and **f** represent possible TIPS results depending on the feed composition, namely single liquid phase (blue, A), L1-L2 (orange, B), S-L phase separation or macroscopic separation (red, D), gelation of the complete volume (green, C).



at low temperatures (Fig. 1b, d). Polymer/solvent/antisolvent mixtures might exhibit a homogeneous liquid area and a liquid–liquid phase separation region as shown in Fig. 1a–d. The binary mixtures polymer/solvent and solvent/antisolvent are both fully miscible. The demixing region originates from the binary polymer/antisolvent mixture and extends into the ternary mixture with the solvent, whereas the addition of the solvent decreases the size of the miscibility gap. All ternary diagrams additionally contain a glass-transition line: Compositions above

that line are glassy, and all compositions below this line are liquid.

Figure 1a and b depicts the phase behavior for a non-crystallizing (amorphous) polymer at high and low temperatures, respectively. For non-crystallizing polymers, only the phase separation region and the glass transition line are relevant for the gel formation process. A gel might be obtained by first dissolving the polymer in a solvent (starting in the homogeneous region on the left side of the diagrams, e.g., Fig. 1a, blue point A) and then cooling the mixture down to lower temperatures (Fig. 1b, green point C).

The polymer-rich and polymer-lean phases are formed and coexist in liquid–liquid equilibrium (orange and green areas in Fig. 1a, b). If this polymer-rich phase is found below its glass transition and is present in sufficient amount, it can form a 3D gel network throughout the whole volume of the sample (Fig. 1b, green region). The entire system thereby loses its ability to flow. We refer to this state as gel formation or gelation. This is precisely the state, which is desirable for aerogel processing.

For a partially crystallizing polymer, Fig. 1c and d needs to be considered. Crystallization now plays a decisive role in gel stabilization besides the phase separation and the glass transition of the polymer/solvent/antisolvent system. Since a polymer does not fully crystallize, there is always residual solvent in the amorphous domains of the polymer and no pure polymer is obtained in a TIPS process: The S-L tie lines do not end in the pure-polymer edge at the top of the triangles but shortly before that. The solvent content in the amorphous parts of the polymer depends on the degree of polymer crystallinity. Thus, these diagrams are only valid for a given degree of polymer crystallinity. For high temperatures, the S-L region might exceed the liquid–liquid equilibrium region (Fig. 1c). Upon decreasing temperature, the latter increases, finally exceeding the S-L region and leading to a three-phase solid–liquid–liquid region (Fig. 1d). In this case, we expect that gelation occurs by overlapping liquid–liquid phase separation and the (partly) crystallization of the polymer-rich phase below its gel transition (upper end of the tie lines located above the glass transition line). As described above, the gel formation in the whole volume of the solution is desired.

The diagrams shown in Fig. 1e and f are obtained by evaluating the ternary solvent/antisolvent/polymer mixtures shown in Fig. 1a, b, and in Fig. 1c, d, respectively, as a function of temperature for one specific solvent/antisolvent ratio (pseudo-binary diagrams). When preparing a gel via TIPS, a polymer is completely dissolved in a solvent or solvent/antisolvent mixture at elevated temperatures (points A and A' in Fig. 1e, f). To induce phase separation, the homogeneous solution is cooled down (indicated by the arrows). The solution could pass different phase separation areas depending on the solvent, polymer type, polymer concentration, and cooling regime. Here, we again differentiate between an amorphous polymer and a semicrystalline one.

### Amorphous polymer (Fig. 1e)

Cooling a homogeneous feed solution of an amorphous polymer with a polymer concentration higher than the critical polymer concentration to temperatures below the binodal curve (Fig. 1e, A to B), the solution forms two phases: a polymer-lean phase and polymer-rich phase (the concentrations of the evolving phases cannot be seen in this diagram anymore). Further cooling of the system below the glass transition temperature (Fig. 1e, B to C) reduces the polymer-chain mobility (*i.e.*, by vitrification). Thus, the L-L phase separation is arrested, leading to a gel with a porous interconnected structure formed by the polymer-rich phase ( $L_2$ ), filled with the polymer-lean phase ( $L_1$ ). Due to the small pore size, the pore liquid  $L_1$  does not flow out even if the gel is turned in any direction. The material appears as one wet body—the gel.

In case the homogeneous feed solution of an amorphous polymer with a polymer concentration below the critical one crosses the binodal upon temperature decrease (Fig. 1e, A'–B'), a polymer-rich dispersed phase ( $L_2$ ) is generated, which will further form a gel at temperatures below glass transition (B'–D'). In this case, the vitrified polymer-rich phase sediments from the solvent-rich phase as a dense phase and might later form an irregular dense gel. This state is undesirable for aerogel production since usually low-density materials are targeted.

### Semicrystalline polymers (Fig. 1f)

Cooling a homogenous solution of a **semicrystalline** polymer, the S-L line is crossed (Fig. 1f, A–D). Here again, two cases are possible. In the first case (A–D), spontaneous precipitation of the polymer-rich phase occurs, leading to the formation of spherulites and eventually to an irregular, poorly interconnected gel [31]. If the cooling process occurs fast, so that the homogeneous solution of the semicrystalline polymer crosses the S-L line followed by crossing the metastable binodal line to the right of the critical polymer concentration (Fig. 1f, A to C), the polymer-rich phase is arrested again and the combination of liquid–liquid phase separation and crystallization yields a desired gel [20, 25].

**Table 1** Properties of polymers PLLA and PDLLA used in this work ( $T_g$  and  $X_{Cr}$ : own measurements)

Name	Brand	D-isomer [mol.%]	$M_w$ [kg mol <sup>-1</sup> ]	$T_g$ [°C]	$X_{Cr}$
PLLA	2500HP, Natureworks	0.4[33]	116[34]	62.2 ± 0.4	32.1% ± 1.1%
PDLLA	4060D, Natureworks	12.0[35]	119[35]	57.3 ± 0.3	0%

## Materials and methods

The polymers PDLLA (amorphous) and PLLA (semicrystalline, Table 1) were investigated in this work. Carbon dioxide with a purity of 99.9% was supplied by Praxair GmbH and was used for the supercritical drying of the prepared gels. Denatured ethanol (ROTH: K928.2) with a concentration greater than 99.8% was used as an antisolvent to gelate PDLLA and solvent exchange step. Dimethyl sulfoxide (DMSO) (ROTH: 7029.5) with a purity greater than 99.5% was used as a solvent for PDLLA. HPLC grade chloroform (ROTH: 7331.1) was used as a solvent for PLLA. HPLC grade methanol (ROTH: 7342.1) was used as an antisolvent for the PLLA gelation.

### Determination of glass transition and degree of crystallinity via differential scanning calorimetry

The  $T_g$  of polymers as a function of CO<sub>2</sub> pressure and presence of ethanol was measured using a Setaram BT 2.15 differential scanning calorimeter (DSC) equipped with high-pressure cells. The measurement and reference cells could be pressurized with CO<sub>2</sub> up to 200 bar. For measuring the influence of CO<sub>2</sub>-ethanol mixtures on the  $T_g$  of the polymers, the polymer was equilibrated inside the measurement cell with CO<sub>2</sub>-saturated ethanol at the specific pressure of the experiment (e.g., 30 bar, 40 bar, etc.) and a temperature of 30 °C (Online Resource, Figure SI1). The Setaram BT 2.15 was calibrated using indium and gallium standards with a 0.2 K min<sup>-1</sup> heating ramp. The same heating ramp was used to determine the glass transition temperatures. Measurements at ambient pressure were performed using a DSC Q2000 device (TA Instruments). All measurements were repeated three times. The degree of crystallinity was determined by relating the PLLA melting enthalpy of the supplied polymer with the melting enthalpy of hypothetically 100% pure PLLA using Eq. 1:

$$X_{Cr} = \frac{\Delta H^{SL}}{\Delta H_{PLLA}^{SL}} \cdot 100 \quad (1)$$

Herein,  $X_{Cr}$  is the degree of crystallinity (%),  $\Delta H^{SL}$  is the melting enthalpy measured via DSC, and  $\Delta H_{PLLA}^{SL}$  is the melting enthalpy of hypothetically 100% crystalline PLLA (93.1 J•g<sup>-1</sup>) [32]. No cold crystallization was observed during the heating ramps of our DSC measurements.

### Gelation process

Gels from amorphous PDLLA and semicrystalline PLLA were produced via the TIPS technique (Table 1). Thereby, two different solvent/antisolvent systems were applied: chloroform–methanol (PLLA, according to the literature and adapted for TIPS [24]) and the DMSO-ethanol system newly proposed in this work (PDLLA). In a stirred closed glass vessel, 40 g of a polymer/solvent/antisolvent feed solution with different compositions was heated to 60 °C (PDLLA) or 70 °C (PLLA) until all compounds were fully dissolved. These temperatures were chosen to avoid the boiling of the solvent/antisolvent/polymer solution. Afterward, the solutions were poured into plastic molds with an internal diameter of 25 mm, hermetically sealed and stored at 25 °C. To increase the cooling rate, some solutions were immediately placed at -20 °C.

### Gelation temperature of polymer–solvent system

Gelation temperature of polymer/solvent mixtures was measured via refractive index measurements using the refractometer Anton Paar Abbemat 300 with an accuracy of ± 0.0001 nD (589 nm) [36]. The refractometer measuring cell was equipped with a Peltier element operating in a temperature range from 5 to 80 °C. During the measurements, the temperature was decreased from 80 to 5 °C in steps of 1 °C at a cooling rate of 2.3 K min<sup>-1</sup>. The sample was

equilibrated for 5 min at every temperature step to assure temperature homogeneity throughout the sample. During the cooling of the solution, two peaks appear. The high-temperature peak represents the cloud point of the solution. The peak at lower temperatures coincides with the gelation of the solution. The gelation temperature was considered as the  $T_{\text{offset}}$  of the low-temperature refractive index peak.

### Supercritical drying of gels

Before supercritical drying of the gels, the solvent/antisolvent mixture inside the pores of the gel was completely exchanged with cold ethanol at  $-20\text{ }^{\circ}\text{C}$  by submerging the gel for 12 h in ethanol (5 g EtOH per gram of gel). This procedure was repeated twice using fresh ethanol. The cold temperature was chosen to be below the  $T_g$  of the antisolvent/polymer system.

For performing the  $\text{scCO}_2$  drying, gels were transferred into a 500-mL autoclave which was equipped with a  $\text{CO}_2$  recirculating unit. First, the ethanol was exchanged by liquid  $\text{CO}_2$  (pressure: 55 bar; temperature:  $-5\text{ }^{\circ}\text{C}$ ; Time: 4 h), followed by simultaneous heating of the autoclave to  $40\text{ }^{\circ}\text{C}$  and increasing the pressure to 100 bar within 1 h. During the entire process, a recirculating flow of  $200\text{ g CO}_2\text{ min}^{-1}$  was maintained with a purging of  $25\text{ g min}^{-1}$  to remove the organic solvents out of the system. After that, depressurization of the autoclave was performed isothermally at  $40\text{ }^{\circ}\text{C}$  and a depressurization rate of  $2\text{ bar min}^{-1}$ . The drying conditions were selected based on standard  $\text{scCO}_2$  drying profiles and to be as close as possible to the  $T_g$  of the polymer. To confirm that the  $\text{scCO}_2$  drying profile works as intended, the volatile content of twelve  $\text{scCO}_2$  dried gels was measured by post-drying them under vacuum at 0.1 mbar and  $60\text{ }^{\circ}\text{C}$ . The average volatile content was determined to be 0.032 wt.%.

The evaporative drying of the gels, which were previously solvent exchanged with ethanol, was performed by evaporating the solvent at room conditions.

All dried gels were finally dried in a vacuum oven at  $25\text{ }^{\circ}\text{C}$ , to remove the organic solvent traces. After the  $\text{scCO}_2$  drying or evaporative drying, the  $\text{N}_2$  BET surface area and the degree of crystallization of the dried gels were measured.

### Measurement of binary phase behavior for PC-SAFT modeling

The demixing zone of the binary PDLLA/ethanol system was quantified gravimetrically. PDLLA pellets were equilibrated with ethanol in a temperature-controlled and stirred vessel (accuracy  $\pm 0.3\text{ }^{\circ}\text{C}$ ). After two days of equilibration, samples were drawn from both phases (triplicate measurements). The polymer concentrations in the polymer-rich and polymer-lean phases were determined via gravimetric determination of solvent loss after complete drying for seven days in a vacuum chamber.

Since the PDLLA/DMSO mixture does not demix, vapor sorption equilibria (V-L) were determined to fit the binary interaction parameters. Therefore, the sorption of DMSO in PDLLA was determined gravimetrically for different DMSO partial pressures using a magnetic suspension balance (Rubotherm, Bochum, Germany) (Online Resource, Figure SI3). The detailed experimental setting was described in earlier work [37]. PC-SAFT binary interaction parameters were fitted to the measured binary phase equilibria data (Online Resource, Figure SI2, and SI3).

### Modeling of phase behavior and glass-transition temperatures

The perturbed-chain statistical associating fluid theory (PC-SAFT) was used to model L-L phase separation for PDLLA-containing mixtures. It is a model for the residual Helmholtz energy  $a^{\text{res}}$ , which considers three different contributions (Eq. 2) [29, 38]:

$$a^{\text{res}} = a^{\text{hc}} + a^{\text{disp}} + a^{\text{assoc}} \quad (2)$$

These are the hard-chain reference contribution  $a^{\text{hc}}$ ,  $a^{\text{disp}}$  which accounts for van der Waals interactions and  $a^{\text{assoc}}$  that accounts for associating interactions (i.e., hydrogen bonds). In PC-SAFT, a molecule is described by 3 pure component parameters, namely the segment number  $m_i^{\text{seg}}$ , the segment diameter  $\sigma_i$  and the dispersion energy parameter  $u_i/k_B$  with  $k_B$  being the Boltzmann constant. Associating molecules require two more parameters, namely the association energy parameter ( $\epsilon_i^{\text{AiBi}}/k_B$ ) and the association volume  $\kappa^{\text{AiBi}}$ . The PC-SAFT pure component parameters of all investigated components are listed in Table 2.

In a mixture, the dispersion energy between molecules  $i$  and  $j$  is obtained using Eq. 3:

**Table 2** PC-SAFT parameters of the substances investigated in this work

	$M$ [g mol <sup>-1</sup> ]	$m_{\text{seg}}/M$ [-]	$\sigma_{\text{seg}}$ [Å]	$u_i/k_B$ [K]	$\varepsilon_i^{\text{AiBi}}/k_B$ [K]	$\kappa^{\text{AiBi}}$ [-]	$N_{\text{assoc}}$ [-]	Source
Ethanol	46.07	2.3827	3.177	198.24	2653.4	0.0324	1/1	[38]
DMSO	78.13	2.9223	3.278	355.69	0	0	–	[39]
PDLLA	113,000	0.03699	3.120	240.0	–	–	–	[40]

$$u_{ij} = (1 - k_{ij}) \cdot \sqrt{u_i \cdot u_j} \quad (3)$$

Herein,  $k_{ij}$  stands for the binary interaction parameter, which may depend linearly on temperature (see Eq. 4):

$$k_{ij}(T) = k_{ij, \text{slope}} \cdot T[\text{K}] + k_{ij, \text{int}} \quad (4)$$

The binary interaction parameters fitted to the binary phase behavior data are summarized in Table 3.

Activity coefficients ( $\gamma_i$ ) were calculated with PC-SAFT using the above-mentioned set of pure-component parameters (Table 2) and binary interaction parameters (Table 3). Activity coefficients consider the intermolecular interactions between molecules in a mixture and allow for calculating the L-L demixing region by solving Eq. 5 for the polymer, solvent and antisolvent ( $x_i$  is the mole fraction of component  $i$  and  $L_1/L_2$  are the two coexisting liquid phases).

$$x_i^{L1} \gamma_i^{L1} = x_i^{L2} \gamma_i^{L2} \quad (5)$$

As an equation of state, PC-SAFT accounts for the entropic effects of mixtures containing components with high differences in molecular weight (polymer vs. solvent). It thus provides the framework to calculate demixing between molecules of different sizes. It should be noted that PC-SAFT does not account for the crystallinity of the polymer. Therefore, it was applied only to amorphous PDLLA and not to semicrystalline PLLA.

Glass transition temperatures were predicted using the Gordon-Taylor equation [30] for ternary mixtures [42] as given in Eq. 6:

$$T_g = \frac{\sum_i K_{\text{polymer},i} w_i T_{g,i}}{\sum_i K_{\text{polymer},i} w_i} \quad (6)$$

In Eq. 6,  $K_{\text{polymer},i}$  are the binary Gordon-Taylor interaction parameters between the other compounds  $i$  and polymer,  $w_i$  are the mass fractions of the individual components, and  $T_{g,i}$  are the glass-transition temperatures of the pure components. The binary Gordon-Taylor interaction parameter  $K_{\text{polymer},i}$  was predicted from the ratio of the densities  $\rho$  and the glass transition temperatures (Eq. 7).

$$K_{\text{polymer},i} = \frac{T_{g,\text{polymer}} \rho_{\text{polymer}}}{T_{g,i} \rho_i} \quad (7)$$

The properties used for the Gordon-Taylor calculations are summarized in Table 4.

The temperature at which the polymer-rich phase exceeds its glass transition was considered as the gelation temperature. For estimating the gel temperatures, L-L demixing was predicted via PC-SAFT solving Eq. 5 for all three components polymer, solvent and antisolvent. Afterward, it was checked by Eq. 6 whether the newly formed polymer-rich phase was above or below its glass transition after demixing.

## Results and discussion

### Gelation phenomena for amorphous polymers: system PDLLA-DMSO-ethanol

PDLLA is considered an amorphous polymer. Thus, we assume that the gelation mechanism is only due to the vitrification of the polymer-rich phase (see Fig. 1a, b and e). Usually, the system methanol/

**Table 3** PC-SAFT interaction parameters for the binary systems investigated in this work

Binary mixture	$k_{ij, \text{slope}}$ [K <sup>-1</sup> ]	$k_{ij, \text{int}}$ [-]	Fitted to data	Temperature range	Ref. for $k_{ij}$
Ethanol/DMSO	–	–0.15	V-L		[41]
PDLLA/ethanol	– 0.00015	0.0275	L-L	25–60 °C	This work
PDLLA/DMSO	–	–0.0200	V-L	77 °C	This work



**Table 4** Glass transition temperatures and densities of the investigated pure components

	$T_g$ [°C]	$\rho$ at 25 °C [kg m <sup>-3</sup> ]	Ref. $T_g$ / $\rho$
Ethanol	- 175.9	789	[43] / [44]
DMSO	- 123.0	1104	[43] / [45]
PDLLA	57.26 ± 0.34	1250	This work / [46]

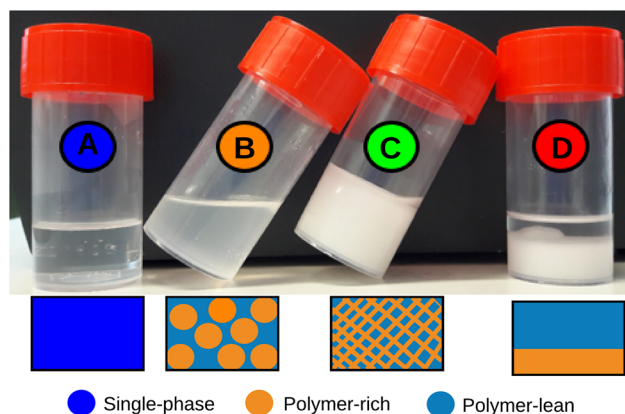


**Figure 2** PDLLA/DMSO/ethanol mixtures showing a different behavior when cooling the corresponding homogeneous solutions from 60 down to 25 °C. The colors represent the different observed states; blue **a**: single phase; orange **b**: phase separation with droplet formation (e.g., droplets of polymer-rich phase in continuous polymer-lean phase or vice versa depending on the composition); green **c**: formation of 3D gel network throughout the whole sample (network is formed out of the polymer-rich phase and filled with polymer-lean phase); red **d**: macroscopic phase separation, no gel formation in polymer-lean phase (top), formation of dispersed and partly aggregated gel particles in polymer-rich phase at the bottom.

chloroform is used for the gelation. As we aim at pharmaceutical applications of aerogels, we suggest here the new solvent/antisolvent system DMSO/ethanol to produce PDLLA aerogels for pharmaceutical applications.

In Fig. 2, the results of visual investigations of initially homogeneous PDLLA/DMSO/ethanol mixtures of different compositions are shown. All mixtures were cooled down from 60 to 25 °C using the procedure described in the materials section. Depending on the initial composition, the mixtures transformed into different states, labeled with colors corresponding to Fig. 1.

Obviously, the state C (gel network formed throughout the whole volume) is desired for further aerogel formation and should be targeted for. To understand the observed behavior, we discuss the different states with the help of phase diagrams presented in Fig. 1.

The behavior of PDLLA/DMSO/ethanol systems upon cooling from 60 to 25 °C is discussed with the help of a pseudo-binary phase diagram (Fig. 1e). The samples whose composition at 25 °C falls in homogeneous areas of the diagram (L1 or L2 in Fig. 1e) yield homogeneous liquid solutions which do not form a gel upon storage at 25 °C (state A in Fig. 2) and thus cannot be used for aerogel processing.

The samples, whose compositions at 25 °C fall in the two-phase area above the  $T_g$  line (area restricted by the binodal and the green dotted curve in Fig. 1e), exhibit droplet formation of the dispersed phase in the continuous phase, without any pronounced gelation phenomena (state B, Fig. 2). Such samples also do not yield any stable gels upon storage and thus cannot be transformed into aerogels. Only in the samples, which compositions fall inside the two-phase area, but below the  $T_g$  line, gelation occurs.

In the green-labeled samples (C), the polymer-rich phase forms a gel network throughout the whole volume of the fluid. The gel formation is assumed to be driven by 2 phenomena: First, spontaneous phase separation in two liquid phases (polymer-lean L1 and polymer-rich L2, state B at Fig. 1e) occurs, and then, the polymer-rich phase is vitrified (transformation in state C, Fig. 1e) leading to the gel formation. The phase ratio between the polymer-rich and polymer-lean phase is an essential factor. Suppose the volume (fraction) of the polymer-rich phase is small. In that case, it cannot form a network throughout the whole volume and rather precipitate as a dense macroscopic phase, which subsequently forms irregular gel structures (state D in Fig. 2 and transformation B' to D' in Fig. 1e).

Pseudo-binary diagrams (Fig. 1e) help to understand the processes yet, do not allow to depict the exact composition of the samples. Thus, we now present the same observations in ternary diagrams at a constant temperature of 25 °C, which was reached as a final system temperature after the cooling process (Fig. 3). The same color labeling as suggested in Fig. 2 is maintained to depict the state of the systems (homogeneous solution, two-phase system, or gel).

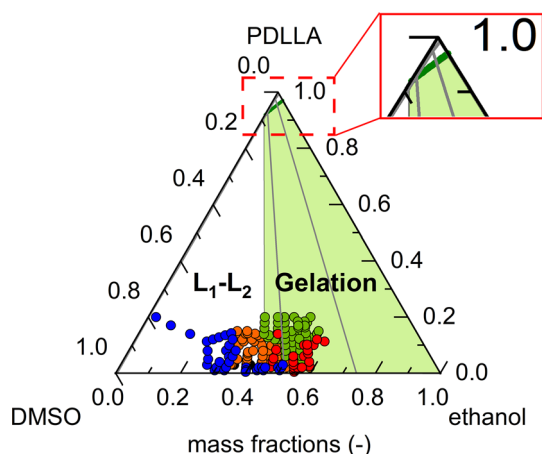


**Figure 3** Ternary diagram for the system PDLLA/DMSO/ethanol at 25 °C. Circles represent the feed compositions of the homogeneous PDLLA/DMSO/ethanol solutions under study; the color of each circle indicates the state of the systems reached upon cooling of the feed solutions, from 60 to 25 °C to: homogeneous liquid (blue), liquid–liquid phase separation (orange), gel formation throughout the volume of the system (green), macroscopic phase separation and gelation of the polymer-rich phase (red). (Physical appearance of the solution is presented in Figure 2 with the same colors.) The gray lines are equilibrium tie lines calculated using PC-SAFT, and the green line is the glass transition composition calculated using the Gordon-Taylor equation.

The solutions with high concentrations of DMSO (> 60 wt.%) and low polymer concentrations (< 20 wt.%) yield homogeneous liquid solutions after cooling (blue symbols), whereas increasing the feed compositions of ethanol (antisolvent) in the PDLLA/DMSO (solvent)/ethanol (antisolvent) system leads to the phase separation (orange dots). Thereby, if the DMSO (solvent) concentration gets lower than 50 wt.%, gelation takes place. Depending on the polymer content and the resulting phase ratio of polymer-rich to polymer-lean phase, either the continuous polymer-rich phase forms a monolithic gel (green points) or the macroscopic phase separation occurs, and the gelation of the lower polymer-rich phase takes place, yielding dense irregular gel (red points).

The equilibria in the system PDLLA/DMSO/ethanol at 25 °C were further modeled by PC-SAFT. According to the PC-SAFT calculation (Fig. 3), the ternary mixture shows a huge miscibility gap. It seems to be an overestimation since experimentally homogeneous solutions (blue dots) were observed in the left part of the predicted phase separation area. Additionally, the glass-transition temperature of the

polymer-rich phase (shown as an inset in Fig. 3) was calculated using Gordon-Taylor. As discussed above (Fig. 1e), the gelation of the amorphous PDLLA is the result of liquid–liquid phase separation and following vitrification of the system upon crossing the glass-transition line of the polymer-rich phase. According to this mechanism, the gelation should occur in the diagram area, where the liquid–liquid phase separation takes place and simultaneously the polymer-rich phase has reached the glassy state. The region in which gelation occurs corresponds to the mixture compositions. Indeed, in the region for which PC-SAFT predicts tie-lines crossing the glass transition line (Fig. 3, green area), all investigated systems formed a gel (either monolithic gel (green dots) or the gel formed after the macroscopic phase separation (red dots)). Note that all dots in Fig. 3 are feed concentrations; the concentrations of both phases after phase separation could not be determined due to gelation phenomena. Thus, this way of thermodynamic modeling enabled the quantification of the phase compositions, being extremely helpful to understand which feed compositions should be targeted to produce the desired gels.

To prove this hypothesis further, gelation temperatures of PDLLA/DMSO/ethanol mixtures at

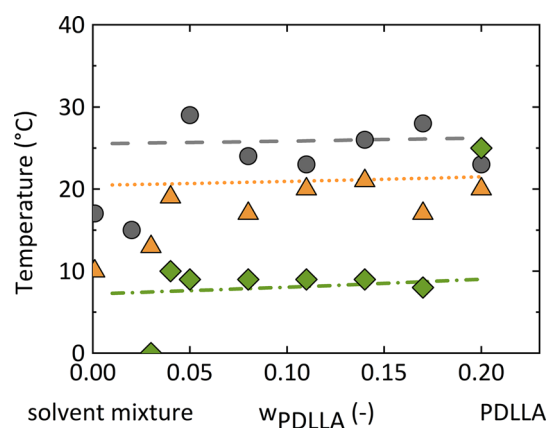


**Figure 4** Gelation temperatures and Tg values of different PDLLA/DMSO/ethanol mixtures. Experimental points were obtained by cooling of the feed samples till gelation occurred (see “Gelation temperature of polymer-solvent system” section); lines are the predicted Tg by the combination of PC-SAFT and the Gordon-Taylor equation. Colors of the symbols and lines correspond to different solvent/antisolvent ratios in the solvent mixture (given as the weight percentage in binary DMSO/ethanol mixture): gray (dashed line/circles)— $w_{\text{DMSO,feed}} = 45$  wt.%; orange (dotted line/triangles)— $w_{\text{DMSO,feed}} = 50$  wt.% and green (dash-dotted line/diamond)— $w_{\text{DMSO,feed}} = 60$  wt.%.

different solvent/antisolvent ratios were measured (Fig. 4) and compared with the  $T_g$  calculated by the combination of PC-SAFT and Gordon-Taylor equation. According to the above mechanism, the gelation should occur once the  $T_g$  is reached. The fraction of DMSO in the DMSO/ethanol mixture was set at 45, 50, and 60 wt%, and the polymer content was chosen to reach the monolithic gels upon cooling (represented quantitatively by the green dots in Fig. 3 and qualitatively by state C in Fig. 1e).

Gelation was observed between 29 °C (for a solution with 45 wt.% DMSO in the feed and an overall PDLLA feed composition of  $w_{PDLLA,feed} = 0.05$ ) and 8 °C (for a solution with 60 wt% DMSO in the feed solvent mixture and an overall PDLLA feed composition of  $w_{PDLLA,feed} = 0.03$ ). The experimental gelation temperatures agree well with the predicted  $T_g$  values (Fig. 4). The gelation temperature slightly increases with increasing PDLLA concentration (e.g.,  $T_{gel}$  increases from 20.5 to 21.5 °C for  $w_{DMSO,feed} = 50$  wt%). In contrast, the higher ratio solvent/antisolvent (DMSO/ethanol) reduces the gelation temperature due to favorable interactions in the system (compatibility polymer–solvent). The polymer concentration has only marginal influence; as the system approaches the critical polymer concentration (PDLLA < 5wt.%), the gelation temperature drops considerably. Thus, we conclude that the prediction of the  $T_g$  of the polymer-rich phase in the system PDLLA/DMSO/ethanol allows us to identify the parameter needed for the gelation process. According to our knowledge, this approach was first applied to discuss the gelation step within the production of polymeric aerogels. Principally, it can be extended to other amorphous polymers.

#### *Gelation phenomena for semicrystalline polymers: PLLA/chloroform/methanol*

The mechanism of the gelation of semicrystalline polymers is different to that of the amorphous ones. Thus, we have investigated whether the methodology described above can be extended to this type of system using the system PLLA/chloroform/methanol (Fig. 1b, d, f). In contrast to the phase behavior of solutions from amorphous polymers, where the PC-SAFT can be applied to the phase equilibrium calculations, the phase equilibrium calculations for a solution from semicrystalline polymers are not possible without considering the semi-crystallinity. An

approach was developed [47, 48] based on the lattice cluster theory (LCT). The LCT accounts only for van der Waals interactions and cannot be applied to the mixtures studied in this investigation.

The gelation of the system PLLA/chloroform/methanol was first studied by van de Witte [23], using the NIPS. In this work, we evaluate the same system using the TIPS technique. Besides the reason of comparison with the PDLLA/DMSO/ethanol system described above, TIPS might result in a higher homogeneity and mesoporous fraction of the gel and thus, in the higher surface area of resulting aerogels. Homogeneous PLLA/chloroform/methanol solutions with different compositions were produced at 70 °C and then slowly cooled down to 25 °C. Only feed compositions at 70 °C below 10 wt.% of PLLA and with a maximum methanol content of 40 wt.% resulted in homogeneous solutions limiting the investigated composition ranges for this system. The results are presented in the ternary diagram (Fig. 5) using the same color code as Fig. 2 for the PDLLA/DMSO/ethanol system. However, the gelation mechanism is different in this case. Since the polymer PLLA is semicrystalline, the crystallization temperature is relevant.

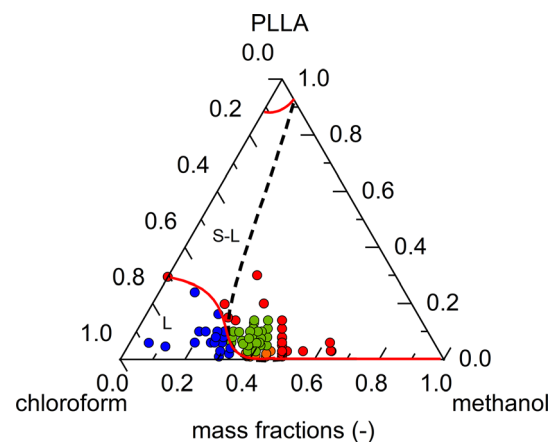


**Figure 5** Ternary diagram for the system PLLA/chloroform/methanol. Circles represent the feed compositions of the homogeneous PLLA/chloroform/methanol under study; the color of each circle indicates the state of the systems reached upon cooling of the feed solutions from 70 to 25 °C: homogeneous liquid (blue), precipitated semicrystalline polymer-rich phase (red), liquid–liquid phase separation (orange) and gel formed throughout the volume of the system (green). The schematic phase behavior as expected according to the experiments is indicated by lines: The black dashed line marks the metastable two-phase region, the red line marks the S-L two-phase region.

To understand the influence of temperature on this process, we refer to Fig. 1f discussed above. When cooling down the homogeneous PLLA/chloroform/methanol (A), two different states can be reached: direct precipitation of the semicrystalline polymer-rich phase (D) or the combination of crystallization and liquid–liquid phase separation yielding monolithic semicrystalline gels occupying the whole volume of the initial mixture (C). The latter state is the desired one for aerogel processing.

Like amorphous PDLLA, a solution of semicrystalline PLLA gels when the polymer-rich phase formed by L-L demixing during the cooling of a homogeneous solution crosses the crystallization line. At the same time, the crystallization of the polymer-rich phase stabilizes the formed structure forming a stable gel occupying the whole volume of the initial solution. When the polymer-rich phase is the continuous phase, an interconnected porous structure, which is characteristic of an aerogel, is formed. The results obtained by this process are shown in Fig. 5 (green dots).

The crystallization of a homogeneous PLLA/chloroform/methanol solution before demixing the system results in the precipitation of the semicrystalline polymer as seen in Fig. 2d and represented in Fig. 5, red dots. The polymer crystallization forms a poorly interconnected structure of spherulites or polycrystalline domain, resulting in a weak gel.

### Influence of supercritical CO<sub>2</sub> drying on the mechanical stability of PLLA and PDLLA-based porous structures

After a stable gel based on PLLA or PDLLA was formed, it should be converted into the corresponding aerogel by supercritical drying. As mentioned in the introduction, supercritical CO<sub>2</sub> (scCO<sub>2</sub>) drying is an important step, which preserves the porous structure of the formed gels. The low T<sub>g</sub> values of the polymer lead to severe difficulties during the drying since the plasticization of the polymer matrix due to the dissolution of CO<sub>2</sub> in the PLA may lead to the loss of the porosity gained initially during the gelation. To understand and quantify the effect of different drying techniques on the material properties and to find a suitable drying protocol, both evaporative drying and scCO<sub>2</sub> drying were performed for the PLLA and PDLLA gels (Fig. 6). As expected, in evaporative drying, a considerable volume shrinkage of the PLLA

and PDLLA gels (Fig. 6b) was observed. (The initial gels had a diameter of 25 mm and a height of 15 mm.) The shrinkage is due to the capillary forces acting on the pore walls when a gas–liquid interface is formed during the evaporation of the solvent inside the pores. To avoid the shrinkage leading to the damage of the mesoporous structure of the gels, scCO<sub>2</sub> drying was performed. In the case of amorphous PDLLA-based gel (Fig. 6c), complete structure loss is observed. In contrast, when supercritical drying was performed on the gels obtained from semicrystalline PLLA, a solid porous structure (aerogel) with no deformations and only minor shrinkage was obtained (Fig. 6d). The morphology of scCO<sub>2</sub> dried aerogels analyzed by SEM (scanning electron microscopy) is shown in the online resource, Figure SI4 to SI6. The SEM pictures show many crystal morphologies and a multi-modal porous structure consisting of pores larger than 1 μm and complex structures characterized by voids smaller than 1 μm.

We suppose that the viscosity of the PDLLA-rich phase forming the gel matrix was significantly reduced during the drying process by increasing the temperature and addition of CO<sub>2</sub>. Thus, the gel structure could not be supported and collapsed, rendering a dense material with no porosity.

It is well known that the glass-transition temperature of the amorphous PDLLA decreases when CO<sub>2</sub> dissolves in it [49, 50]. The gel contains not only the polymer but also solvents, and thus, the interaction of CO<sub>2</sub> with the multicomponent polymer–solvent mixture needs to be understood. In Fig. 7, the effect of pure CO<sub>2</sub> and a binary CO<sub>2</sub> + ethanol mixture on the T<sub>g</sub> of PDLLA (this work) and on the polymer with a 4.2% D-isomer content [49] is shown. Both polymers have a molar mass above the critical molar mass (> 10 kDa); thus, the molecular weight of the polymer has only an extremely small influence on the glass transition temperature. The T<sub>g</sub> is reduced with increasing CO<sub>2</sub> pressure in all cases due to the dissolution of CO<sub>2</sub> into the polymer phase. The addition of ethanol to the system does not change this behavior.

It should be noted that measuring the T<sub>g</sub> of the polymer close to or above the critical pressure of the carbon dioxide (31 °C, 71 bar) is difficult due to the exothermal peak produced by the CO<sub>2</sub> phase transition from the gas phase to the supercritical phase when measuring with DSC techniques [49]. It is

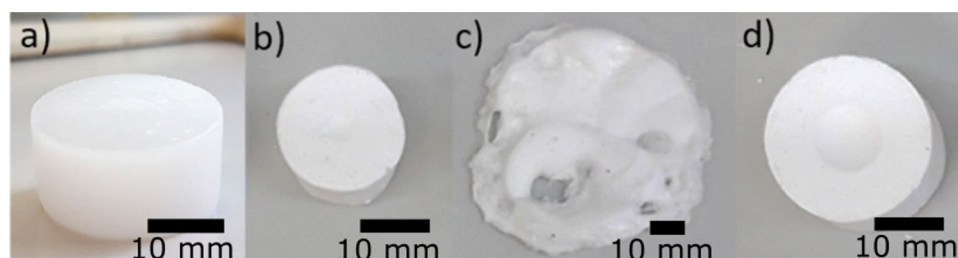


**Figure 6** Photographs gels and aerogels: **a** initial PLLA (semicrystalline) wet gel, **b** PLLA gel dried via evaporative drying, **c** PDLLA (amorphous) gel supercritically dried and **d** PLLA gel supercritically dried.

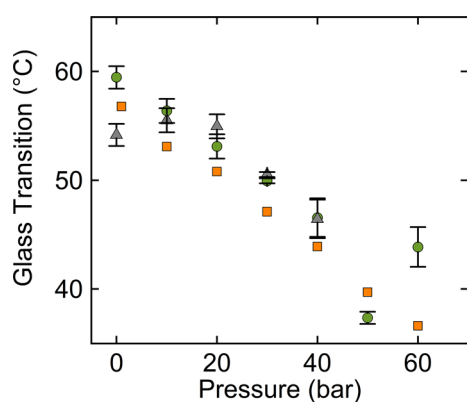


**Figure 7** Glass transition temperatures of polymers as a function of CO<sub>2</sub> pressure. Orange squares: CO<sub>2</sub>-PDLLA taken from literature (4.2 mol% D-isomer in PDLLA); green circles: CO<sub>2</sub>-PDLLA (12 mol% D-isomer in PDLLA); and gray triangles: are the values for CO<sub>2</sub>-PDLLA-Ethanol (12 mol% D-isomer in PDLLA). CO<sub>2</sub> concentration in the liquid phase corresponds to the equilibrium solubility value at 30 °C and pressure of the experiment (Online Resource, Figure S11) [49].

expected that the T<sub>g</sub> of the polymer continuously depreciates with increasing pressure until retrograde vitrification occurs [51].

The glass-transition temperature of the polymer matrix is an essential factor to consider when processing polymeric gels with CO<sub>2</sub> at high pressures. To avoid the softening of the polymer structure (Fig. 6c), several authors advise performing the supercritical drying process below the glass-transition temperature of the polymer and performing the drying between 35 and 40 °C [6, 12]. All scCO<sub>2</sub> processes operate at a minimum pressure of 73.5 bar. As seen in Fig. 7, even at temperatures as low as 31 °C (critical temperature of pure CO<sub>2</sub> and thus the minimum theoretical drying temperature), there is no combination of pressure and temperature that allows operating a scCO<sub>2</sub> process below the T<sub>g</sub> of the polymer.

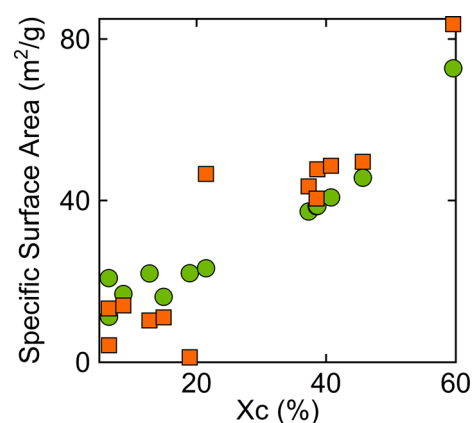


**Figure 8** Surface area of PLA porous structures after evaporative or supercritical drying as a function of crystallinity. Orange squares: scCO<sub>2</sub> drying. Green circles: evaporative drying. Polymers used: PDLLA (X<sub>c</sub> < 25%) and PLLA (X<sub>c</sub> > 25%).

The semi-crystallinity of the polymer also plays a vital role during the process. On the one hand, increasing the semi-crystallinity of the polymer increases the T<sub>g</sub> slightly. On the other hand, the crystalline fraction of the polymer can stabilize the porous structure. In Fig. 8, the BET surface area of semicrystalline PLLA (X<sub>c</sub> > 25%) and amorphous PDLLA (X<sub>c</sub> < 25%) gels after evaporative drying and scCO<sub>2</sub> drying correspondingly is plotted against the degree of crystallinity of the final solid material. The scattering of the BET surface area can be attributed to the inhomogeneous structure formed during the kinetic cooling of the polymer/solvent/non-solvent solutions. A higher value of the specific surface area is traditionally explained by a larger mesoporous fraction, preserved during the scCO<sub>2</sub> drying and destroyed during the evaporative drying. Indeed, all gels with a crystallinity degree below 25% were collapsed after the supercritical drying process (Fig. 6c). In contrast, the gels with a polymer crystallinity degree above 25% show no evident macroscopic

damages (Fig. 6d). As shown in Fig. 8 gels with low crystallinity (below 25%) lead to higher specific surface areas after evaporative drying than the scCO<sub>2</sub> drying. On the other hand, the gels with high crystallinity (above 25%) show a higher value on the specific surface area when dried using scCO<sub>2</sub>. The crystallinity of the polymer is an important factor.

Besides the crystallinity itself, the pore size distribution should be considered: The porous gel structure formed by the TIPS technique contains a mixture of mesopores and macropores. The low specific surface areas and the minor differences between the specific surface area of supercritically dried and evaporative-dried gels indicate that there is a large fraction of macropores (> 500 nm), which have less contribution to the surface area. Since the capillary force is inversed proportional to the pore size, macropores are less prone to pore collapse during the drying. Therefore, the results of evaporative drying and scCO<sub>2</sub> drying get closer to each other.

Further, the polymer crystallinity of the gel influences its rheological properties, which change significantly during the dissolution of CO<sub>2</sub> in the polymer (plasticization). Generally, when a polymer is plasticized (by means of temperature or addition of a plasticizer), the storage modulus of the material beyond the glass transition temperature is decreased. Tabí Et al. [52] measured the storage modulus of both crystalline and amorphous polymers as a function of temperature. In the case of the amorphous PDLLA, when the temperature approaches the glass transition temperature, the storage modulus tends to zero, due to the viscosity reduction of the amorphous domain. The storage modulus of a PLLA with a higher crystallinity is less affected by temperature, especially when the temperature is above the glass transition temperature. The storage modulus is related to the rheological behavior of the porous structure. If the storage modulus is low, the porous structure collapses by its own weight explaining the results obtained for the low crystallinity gels (Fig. 6c). In the case of a semicrystalline polymer, which is composed of amorphous and crystalline domains, the crystallites whose melting temperature at the drying conditions (CO<sub>2</sub> pressures above 60 bar) is larger than 100 °C [53] act as a backbone supporting the porous structure when the viscosity of the amorphous domain is reduced. That is why a minimum number of crystallites (in our experiments  $X_c > 25\%$ ) is

required to stabilize the structure during the scCO<sub>2</sub> drying procedure, as shown in Fig. 8.

Since the polymer crystallinity reduces the effect that the temperature and plasticizers have on the storage modulus, we conclude that it is the main factor that needs to be controlled to enable the processing of porous PLA materials with scCO<sub>2</sub>.

### Controlling the crystallinity degree of the PLLA gels

Since crystallinity plays a vital role in the drying process, the question arises if it can be tailored during the gelation process itself.

Since the TIPS technique in semicrystalline polymers can be regarded as an annealing process, the final crystallinity degree can be controlled during the gelation. Increasing the crystallinity enables the scCO<sub>2</sub> drying and controls the rheological and thermal properties and the degradability.

Different parameters can control the crystallinity during the TIPS process: the solvent/antisolvent ratio, polymer concentration and initial polymer type. In the case of the semicrystalline PLLA, the initial composition of the system has an important effect on the final polymer crystallinity. In Fig. 9, the crystallinity of the gels obtained by the TIPS process in the system PLLA/methanol/chloroform at two different polymer contents is shown as a function of the feed composition. Firstly, the crystallinity increases with increasing antisolvent (chloroform) content for both polymer concentrations in the

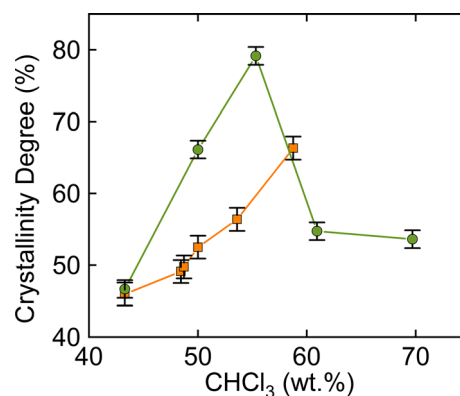


**Figure 9** Effect of solvent composition on the crystallinity degree of PLLA-based porous structures at two polymer concentrations. Green circles: 6 wt.% of PLLA in the feed solution. Orange squares: 3 wt.% of PLLA in the feed solution. Lines guide the reader's eye.

system. A maximum polymer crystallinity was achieved with a chloroform feed composition between 55 and 61 wt.%. The following decrease in the crystallinity can be explained considering the gelation mechanism discussed in Fig. 2f. If the gelation occurs due to direct crystallization out of the homogeneous solution (process A-D in Fig. 2f), the crystallinity of the polymer increases as the fraction of solvent in the feed increases. If the separation occurs by a combination of liquid-liquid phase separation and crystallization (process A-C at Fig. 2f), the solvent/antisolvent ratio has almost no impact on the final crystallinity of the polymer. The latter case explains the plateau of crystallinity at polymer and high antisolvent concentrations (green circles at methanol concentration above 55%). It should be noted that in all cases, the crystallinity was high enough so that all these PLLA gels withstood the scCO<sub>2</sub> drying process without signs of shrinkage or deformation.

Even though PDLLA is considered an amorphous polymer, we found out that the gelation through TIPS induces some crystallinity due to the annealing effect of the process (Fig. 9). The crystallinity degree of the porous polymer is significantly lower compared to PLLA, leading to almost amorphous gels [53]. In all experiments with PDLLA, only crystallinity within the range 0% to 16.4% was reached. Accordingly, all the gels prepared with PDLLA collapsed during the scCO<sub>2</sub> drying, supporting the importance of the polymer crystallinity induced during the gelation to enable the scCO<sub>2</sub> drying.

### Measures to increase the surface area of aerogels

#### Modification of supercritical drying process

Although a better understanding of the influence of crystallinity and plasticizing effects on the surface area was reached in this work, we still observe that the surface areas in all investigated cases are still much lower, as those which can be achieved with other polymers (85 m<sup>2</sup> g<sup>-1</sup> (Fig. 8) vs. typical values of 300–500 m<sup>2</sup> g<sup>-1</sup>).

To overcome the plasticizing effect of ethanol and scCO<sub>2</sub>, we suggest introducing an additional step before the supercritical drying: solvent exchange of ethanol-containing gel with liquid CO<sub>2</sub> at low temperature. First, the gelation solvents are exchanged

**Table 5** Specific surface areas of supercritically dried PLLA gels with two types of solvent exchange

Polymer wt.%	BET Surface Area, m <sup>2</sup> g <sup>-1</sup>	
	Ethanol	Ethanol + Liquid CO <sub>2</sub>
6	59.6	74.1
8	59.1	68.7
10	56.7	66.0

(1) ethanol. (2) ethanol followed by liquid CO<sub>2</sub>. Content of chloroform in the solvent mixture = 66,7 wt%

with ethanol (antisolvent for PLLA and PDLLA) to completely vitrify and crystallize the polymer-rich phase of the produced PLA gels. Then, according to our suggestion, the ethanol contained inside the pores of the gel is exchanged with liquid CO<sub>2</sub> and then the scCO<sub>2</sub> drying is applied. In Table 5, the differences in specific surface area of dried aerogels with different polymer concentrations, which underwent the liquid CO<sub>2</sub> treatment along with those of reference aerogels (without liquid CO<sub>2</sub> treatment), are shown. The suggested ethanol exchange with liquid CO<sub>2</sub> at low temperatures (−5 °C) helps reduce the polymer network damage due to the high plasticizing effect of the mixture ethanol with scCO<sub>2</sub> allowing for slightly higher surface areas. We assume that by replacing the ethanol with liquid CO<sub>2</sub> at low temperatures (−5 °C) and low pressures (55 bar) followed by the supercritical drying at 40 °C and 100 bar, the storage modulus of the polymeric network is maximized. However, the increase in specific surface area is not as pronounced as we hoped.

#### Modification of gelation conditions: gel content and quenching time

Generally, the specific surface area of the dried PLLA porous materials depends also on the gelation. The cooling rate of the solution plays an important role in the final pore size and the crystalline structure. Due to the coalescence of the phases, the longer the time a solution spends inside the L-L two-phase region, the higher is the loss of the initial structure. Thus, the pore size of the final material is inversely proportional to the time which the system spends inside the L-L two-phase region and the solidification of the polymer-rich phase ( $t_{\text{gel}}$ ). Consequently, it is necessary to limit the extent of coalescence by reducing the

**Table 6** BET surface areas of PLA aerogels obtained from homogeneous solutions of PLLA quenched at 25 °C and –20 °C and dried under scCO<sub>2</sub> as a function of polymer composition content of chloroform in the solvent mixture = 66,7 wt%

Polymer, wt. %	BET Surface Area, m <sup>2</sup> g <sup>-1</sup>	
	25 °C	– 20 °C
6	33.5	74.1
8	34.9	68.8
10	29.2	66.0

time the mixture spends inside the L-L two-phase region, for instance, by quenching. The effect that quenching of the homogeneous solutions of PLLA has on the final specific surface area is shown in Table 6. The increase in the specific surface area is attributed to the reduction in the pore size (formation of mesopores), since a deeper quench (smaller  $t_{\text{gel}}$ ) reduces the probability of coalescence events.

The solvent/antisolvent ratio and the polymer concentration modify mainly the structure morphology [54]. In Fig. 10, the specific surface area for the supercritically dried PLLA-gels with different solvent compositions and polymer concentrations is presented.

The influence of the solvent content on the specific surface area is larger than the influence of the polymer content, as seen in Fig. 10. Increasing the solvent content on the system leads to larger specific surfaces

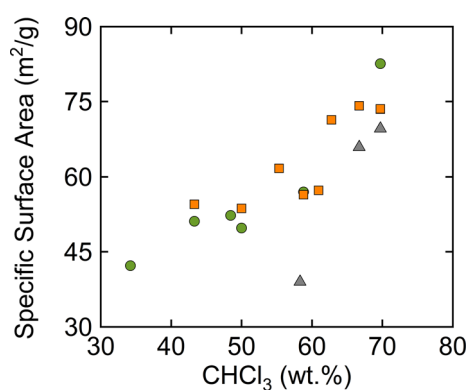


**Figure 10** BET surface area of supercritically dried PLLA gels as a function of polymer content and chloroform concentration in the solvent system. Green circles: 3 wt.% of PLLA as feed composition. Orange squares: 6 wt.% of PLLA in feed composition. Gray triangles: 10 wt. % of PLLA in feed composition. Gelation by quenching to –20 °C and scCO<sub>2</sub> was performed using liquid CO<sub>2</sub> + scCO<sub>2</sub>.

areas, but also the crystallinity degree of the polymer is affected, as depicted in Fig. 9. Even though the crystallites might contribute to the specific surface area, the main contributor is the mesoporous structure of the obtained aerogel. Thus, it is evident that for all the PLLA gels with a crystallinity degree above 25%, increasing the chloroform content results in a higher fraction of mesopores.

### Guidelines to produce low T<sub>g</sub> polymer aerogels

Based on the results of this work, the following guidelines to produce aerogels out of polymers with low T<sub>g</sub> (in this case, PLLA and PDLA) using scCO<sub>2</sub> drying can be derived.

1. Carbon dioxide is highly soluble in semicrystalline and amorphous polymers; thus, the viscosity of the amorphous polymer domain is reduced during the supercritical drying of the polymer gels. For the polymer to withstand the supercritical drying process, a minimum polymer crystallinity termed as critical crystallinity is required, as shown in Figs. 6 and 8 (identified as 25% in the present work).
2. Depending on the final application of the polymeric aerogel, the crystallinity of the polymeric gel can be adjusted between the critical crystallinity and the maximum crystallinity by choosing an appropriate solvent/antisolvent ratio and the copolymer type.
3. The combined effect of high-pressure CO<sub>2</sub> and antisolvent (ethanol) at the beginning of the supercritical drying reduces the storage modulus of the polymer. It is recommended to perform a solvent exchange with liquid CO<sub>2</sub> at low temperatures (–5 °C) to remove all antisolvent traces before increasing the pressure and temperature to supercritical conditions.
4. Increasing the solvent amount on the polymer/solvent/antisolvent system and reducing the gelation time (quenching) maximizes the formation of mesopores.



## Conclusion

In this work, we aimed to improve the understanding of aerogel production based on semicrystalline and amorphous polymers (PLLA and PDLLA) using thermodynamic analysis of the corresponding gelation processes and different types of drying. For that, we extended the previously studied gelation region in the system PLLA/CH<sub>3</sub>Cl/methanol in comparison with the data already available in the literature [24]. We suggested an alternative gelation system PDLLA/DMSO/ethanol to enable the pharmaceutical applications of the resulted aerogels. It was shown that the knowledge of the phase equilibria: liquid–liquid equilibria in amorphous polymers and the superposition of liquid–liquid and solid–liquid equilibria for semicrystalline polymers, together with the glass transition of the corresponding polymer-rich phases, help to identify the compositions of the feed mixtures, leading to the desired gelation behavior. Thereby, in the case of amorphous polymers, it was possible to predict the phase compositions by PC-SAFT. Combining the prediction of the tie-lines and the calculation of T<sub>g</sub> with Gordon-Taylor equation allowed for deeper understanding and even a semi-quantitative description of the gelation process. For semicrystalline polymers further modeling allowing for the consideration of the degree of crystallinity is still needed.

Both evaporative drying and supercritical drying of the resulted PLLA and PDLLA gels were performed. In the case of scCO<sub>2</sub> drying, it was clearly shown that there is no possible combination of pressure and temperature which allows operating the process below the T<sub>g</sub> of the polymer. Thus, in the case of amorphous polymers, supercritical drying would result in the structure collapse in all cases. Though inducing crystallinity in the gel helps to avoid the structure collapse, a minimum crystallinity degree of 25% together with a second solvent exchange with liquid CO<sub>2</sub> before the drying process allows to achieve aerogels with BET surface areas up to 85 m<sup>2</sup> g<sup>-1</sup>. Based on this study, some guidelines for producing aerogels from polymers with low T<sub>g</sub> were formulated. Still, the achieved surface area is significantly lower than aerogels based on other polymers (e.g., alginate, starch), indicating the need for further research in this area.

## Acknowledgements

This research was supported by the Deutsche Forschungsgemeinschaft, DFG, project number SM 82/16-1, SA 700/22-1 and EN 291-10-1.

## Funding

Open Access funding enabled and organized by Projekt DEAL.

## Declarations

**Conflict of interest** The authors declare that there is no conflict of interest associated with this research.

**Supplementary Information:** The online version contains supplementary material available at <http://doi.org/10.1007/s10853-021-06501-0>.

**Open Access** This article is licensed under a Creative Commons Attribution 4.0 International License, which permits use, sharing, adaptation, distribution and reproduction in any medium or format, as long as you give appropriate credit to the original author(s) and the source, provide a link to the Creative Commons licence, and indicate if changes were made. The images or other third party material in this article are included in the article's Creative Commons licence, unless indicated otherwise in a credit line to the material. If material is not included in the article's Creative Commons licence and your intended use is not permitted by statutory regulation or exceeds the permitted use, you will need to obtain permission directly from the copyright holder. To view a copy of this licence, visit <http://creativecommons.org/licenses/by/4.0/>.

**Supplementary Information:** The online version contains supplementary material available at <http://doi.org/10.1007/s10853-021-06501-0>.

## References

- [1] Soleimani Dorcheh A, Abbasi MH (2008) Silica aerogel; synthesis, properties and characterization. *J Mater Process Technol* 199:10–26. <https://doi.org/10.1016/j.jmatprotec.2007.10.060>

- [2] Gurikov P, Raman SP, Weinrich D, Fricke M, Smirnova I (2015) A novel approach to alginate aerogels: carbon dioxide induced gelation. *RSC Adv* 5:7812–7818. <https://doi.org/10.1039/C4RA14653K>
- [3] Gavillon R, Budtova T (2008) Aerocellulose: new highly porous cellulose prepared from cellulose–NaOH aqueous solutions. *Biomacromol* 9:269–277. <https://doi.org/10.1021/bm700972k>
- [4] Paraskevopoulou P, Chriti D, Raptopoulos G, Anyfantis GC (2019) Synthetic polymer aerogels in particulate form. *Materials* 12:1543–1567. <https://doi.org/10.3390/ma12091543>
- [5] Cardea S, Baldino L, Scognamiglio M, Reverchon E (2014) 3D PLLA/Ibuprofen composite scaffolds obtained by a supercritical fluids assisted process. *J Mater Sci: Mater Med* 25:989–998. <https://doi.org/10.1007/s10856-013-5130-z>
- [6] Salerno A, Domingo C (2014) Making microporous nanometre-scale fibrous PLA aerogels with clean and reliable supercritical CO<sub>2</sub> based approaches. *Microporous and Mesoporous Mater* 184:162–168. <https://doi.org/10.1016/j.micromeso.2013.10.019>
- [7] Sun X, Xue B, Tian Y, Qin S, Xie L (2018) 3D porous poly(L-lactic acid) materials with controllable multi-scale microstructures and their potential application in oil-water separation. *Appl Surf Sci* 462:633–640. <https://doi.org/10.1016/j.apsusc.2018.08.119>
- [8] Rezabeigi E, Wood-Adams PM, Drew RAL (2014) Production of porous polylactic acid monoliths via non-solvent induced phase separation. *Polymer (United Kingdom)* 55:6743–6753. <https://doi.org/10.1016/j.polymer.2014.10.063>
- [9] Nam YS, Park TG (1999) Biodegradable polymeric microcellular foams by modified thermally induced phase separation method. *Biomaterials* 19:1783–1790. [https://doi.org/10.1016/S0142-9612\(99\)00073-3](https://doi.org/10.1016/S0142-9612(99)00073-3)
- [10] Scherdel C, Reichenauer G, Wiener M (2010) Relationship between pore volumes and surface areas derived from the evaluation of N<sub>2</sub>-sorption data by DR- BET- and t-plot. *Microporous Mesoporous Mater* 132:572–575. <https://doi.org/10.1016/j.micromeso.2010.03.034>
- [11] Chen J-S, Tu S-L, Tsay R-Y (2010) A morphological study of porous polylactide scaffolds prepared by thermally induced phase separation. *J Taiwan Inst Chem Eng* 41:229–238. <https://doi.org/10.1016/j.jtice.2009.08.008>
- [12] Reverchon E, Cardea S, Rapuano C (2008) A new supercritical fluid-based process to produce scaffolds for tissue replacement. *J Supercrit Fluids* 45:365–373. <https://doi.org/10.1016/j.supflu.2008.01.005>
- [13] Rezabeigi E, Drew RAL, Wood-Adams PM (2017) Highly porous polymer structures fabricated via rapid precipitation from ternary systems. *Ind Eng Chem Res* 56:11451–11459. <https://doi.org/10.1021/acs.iecr.7b02786>
- [14] Hua FJ, Kim GE, Lee JD, Son YK, Lee DS (2002) Macroporous poly(L-lactide) scaffold 1. Preparation of a macroporous scaffold by liquid-liquid phase separation of a PLLA-dioxane-water system. *J Biomed Mater Res A* 63:161–167. <https://doi.org/10.1002/jbm.10121>
- [15] Yang F, Murugan R, Ramakrishna S, Wang X, Ma Y-X, Wang S (2004) Fabrication of nano-structured porous PLLA scaffold intended for nerve tissue engineering. *Biomaterials* 25:1891–1900. <https://doi.org/10.1016/j.biomaterials.2003.08.062>
- [16] He L, Zhang Y, Zeng X, Quan D, Liao S, Zeng Y, Lu J, Ramakrishna S (2009) Fabrication and characterization of poly(L-lactic acid) 3D nanofibrous scaffolds with controlled architecture by liquid–liquid phase separation from a ternary polymer–solvent system. *Polymer* 50:4128–4138. <https://doi.org/10.1016/j.polymer.2009.06.025>
- [17] Shao J, Chen C, Wang Y, Chen X, Du C (2012) Early stage structural evolution of PLLA porous scaffolds in thermally induced phase separation process and the corresponding biodegradability and biological property. *Polym Degrad Stab* 97:955–963. <https://doi.org/10.1016/j.polymdegradstab.2012.03.014>
- [18] A. C, Olivás-Armendariz I, S. J, E. P (2011) Scaffolds for Tissue Engineering Via Thermally Induced Phase Separation. In: Wislet-Gendebien S. *Advances in Regenerative Medicine 1<sup>st</sup> Ed.* InTech
- [19] Salerno A, Fernández-Gutiérrez M, Román S, del Barrio J, Domingo C (2015) Bio-safe fabrication of PLA scaffolds for bone tissue engineering by combining phase separation, porogen leaching and scCO<sub>2</sub> drying. *J Supercrit Fluids* 97:238–246. <https://doi.org/10.1016/j.supflu.2014.10.029>
- [20] Lloyd DR, Kim SS, Kinzer KE (1991) Microporous membrane formation via thermally-induced phase separation. II. Liquid–liquid phase separation. *J Membr Sci* 64:1–11. [https://doi.org/10.1016/0376-7388\(91\)80073-F](https://doi.org/10.1016/0376-7388(91)80073-F)
- [21] Önder ÖC, Yilgör E, Yilgör I (2016) Fabrication of rigid poly(lactic acid) foams via thermally induced phase separation. *Polymer (United Kingdom)* 107:240–248. <https://doi.org/10.1016/j.polymer.2016.11.025>
- [22] van de Witte P, Boorsma A, Esselbrugge H, Dijkstra PJ, van den Berg JWA, Feijen J (1996) Differential scanning calorimetry study of phase transitions in poly(lactide)–chloroform–methanol systems. *Macromolecules* 29:212–219. <https://doi.org/10.1021/ma950300e>
- [23] van de Witte P, Esselbrugge H, Dijkstra PJ, van den Berg JWA, Feijen J (1996) Phase transitions during membrane formation of polylactides. I. A morphological study of membranes obtained from the system polylactide–

- chloroform-methanol. *J Membr Sci* 113:223–236. [https://doi.org/10.1016/0376-7388\(95\)00068-2](https://doi.org/10.1016/0376-7388(95)00068-2)
- [24] van de Witte P, Dijkstra PJ, van den Berg JWA, Feijen J (1996) Phase behavior of polylactides in solvent-nonsolvent mixtures. *J Polym Sci B Polym Phys* 34:2553–2568. [http://doi.org/10.1002/\(SICI\)1099-0488\(19961115\)34:15%3c2553::AID-POLB3%3e3.0.CO;2-U](http://doi.org/10.1002/(SICI)1099-0488(19961115)34:15%3c2553::AID-POLB3%3e3.0.CO;2-U)
- [25] van de Witte P, Dijkstra PJ, van den Berg JWA, Feijen J (1996) Phase separation processes in polymer solutions in relation to membrane formation. *J Membr Sci* 117:1–31. [https://doi.org/10.1016/0376-7388\(96\)00088-9](https://doi.org/10.1016/0376-7388(96)00088-9)
- [26] Gay S, Lefebvre G, Bonnin M, Nottelet B, Boury F, Gibaud A, Calvignac B (2018) PLA scaffolds production from thermally induced phase separation: effect of process parameters and development of an environmentally improved route assisted by supercritical carbon dioxide. *J Supercrit Fluids* 136:123–135. <https://doi.org/10.1016/j.supflu.2018.02.015>
- [27] Şahin İ, Özbakır Y, İnönü Z, Ulker Z, Erkey C (2017) Kinetics of supercritical drying of gels. *Gels* 4:3–32. <https://doi.org/10.3390/gels4010003>
- [28] Chen V, Ma P (2006) The effect of surface area on the degradation rate of nano-fibrous poly(l-lactic acid) foams. *Biomaterials* 27:3708–3715. <https://doi.org/10.1016/j.biomaterials.2006.02.020>
- [29] Gross J, Sadowski G (2001) Perturbed-chain SAFT: an equation of state based on a perturbation theory for chain molecules. *Ind Eng Chem Res* 40:1244–1260. <https://doi.org/10.1021/ie0003887>
- [30] Gordon M, Taylor JS (2007) Ideal copolymers and the second-order transitions of synthetic rubbers. i. non-crystalline copolymers. *J Appl Chem* 2:493–500. <https://doi.org/10.1021/jctb.5010020901>
- [31] Lloyd DR, Kinzer KE, Tseng HS (1990) Microporous membrane formation via thermally induced phase separation. I Solid-liquid phase separation. *J Membr Sci* 52:239–261. [https://doi.org/10.1016/S0376-7388\(00\)85130-3](https://doi.org/10.1016/S0376-7388(00)85130-3)
- [32] Tsuji H, Ikada Y (1996) Crystallization from the melt of poly(lactide)s with different optical purities and their blends. *Macromol Chem Phys* 197:3483–3499. <https://doi.org/10.1002/macp.1996.021971033>
- [33] Jauzein T, Huneault MA, Heuzey M-C (2017) Crystallinity and mechanical properties of polylactide/ether-amide copolymer blends. *J Appl Polym Sci* 134:14–24. <https://doi.org/10.1002/app.44677>
- [34] McKeown P, McCormick SN, Mahon MF, Jones MD (2018) Highly active Mg<sub>2</sub> and Zn<sub>2</sub> complexes for the ring opening polymerization of lactide. *Polym Chem* 9:5339–5347. <http://doi.org/10.1039/C8PY01369A>
- [35] Puchalski M, Kwolek S, Szparaga G, Chrzanowski M, Krucińska I (2017) Investigation of the influence of PLA molecular structure on the crystalline forms ( $\alpha'$  and  $\alpha$ ) and mechanical properties of wet spinning fibres. *Polymers* 9:18–31. <https://doi.org/10.3390/polym9010018>
- [36] Mohsen-Nia M, Rasa H, Modarress H (2006) Cloud-point measurements for (Water + Poly(ethylene glycol) + Salt) ternary mixtures by refractometry method. *J Chem Eng Data* 51:1316–1320. <https://doi.org/10.1021/je060061y>
- [37] Krüger K-M, Sadowski G (2005) Fickian and non-fickian sorption kinetics of toluene in glassy polystyrene. *Macromolecules* 38:8408–8417. <https://doi.org/10.1021/ma050353o>
- [38] Gross J, Sadowski G (2002) Application of the perturbed-chain SAFT equation of state to associating systems. *Ind Eng Chem Res* 41:5510–5515. <https://doi.org/10.1021/ie010954d>
- [39] Gross J, Vrabec J (2006) An equation-of-state contribution for polar components: dipolar molecules. *AIChE J* 52:1194–1204. <https://doi.org/10.1002/aic.10683>
- [40] Cocchi G, Angelis MGD, Sadowski G, Doghieri F (2014) Modelling polylactide/water/dioxane systems for TIPS scaffold fabrication. *Fluid Phase Equilib* 374:1–8. <https://doi.org/10.1016/j.fluid.2014.04.007>
- [41] Caßens J (2013) Modellierung thermodynamischer Eigenschaften pharmazeutischer Substanzen in Lösungsmitteln und Lösungsmittelgemischen. Technische Universität Dortmund
- [42] Lehmkemper K, Kyeremateng SO, Heinzerling O, Degenhardt M, Sadowski G (2017) Long-term physical stability of PVP- and PVPVA-amorphous solid dispersions. *Mol Pharmaceutics* 14:157–171. <https://doi.org/10.1021/acs.molpharmaceut.6b00763>
- [43] Lesikar AV (1977) On the glass transition in mixtures between the normal alcohols and various Lewis bases. *J Chem Phys* 66:4263–4276. <https://doi.org/10.1063/1.433736>
- [44] Takiguchi Y, Uematsu M (1996) Densities for liquid ethanol in the temperature range from 310 K to 480 K at pressures up to 200 MPa. *J Chem Thermodyn* 28:7–16. <https://doi.org/10.1006/jcht.1996.0003>
- [45] LeBel RG, Goring DAI (1962) Density, viscosity, refractive index, and hygroscopicity of mixtures of water and dimethyl sulfoxide. *J Chem Eng Data* 7:100–101. <https://doi.org/10.1021/je60012a032>
- [46] Di Lorenzo ML, Androsch R (2019) Thermal properties of bio-based polymers. Springer International Publishing, Cham
- [47] Fischlschweiger M, Enders S (2014) A theory for solubility of semicrystalline and branched polymers in one solvent.

Macromolecules 47:7625–7636. <https://doi.org/10.1021/ma501440x>

- [48] Fischlschweiger M, Enders S (2014) Solid–liquid equilibria of crystalline and semicrystalline monodisperse polymers, taking into account the molecular architecture by application of the lattice cluster theory. *Mol Phys* 112:3109–3119. <https://doi.org/10.1080/00268976.2014.931605>
- [49] Huang E, Liao X, Zhao C, Park CB, Yang Q, Li G (2016) Effect of unexpected CO<sub>2</sub>'s phase transition on the high-pressure differential scanning calorimetry performance of various polymers. *ACS Sustain Chem Eng* 4:1810–1818. <https://doi.org/10.1021/acssuschemeng.6b00008>
- [50] Nofar M, Ameli A, Park CB (2014) The thermal behavior of polylactide with different D-lactide content in the presence of dissolved CO<sub>2</sub>. *Macromol Mater Eng* 299:1232–1239. <https://doi.org/10.1002/mame.201300474>
- [51] Condo PD, Johnston KP (1994) In situ measurement of the glass transition temperature of polymers with compressed fluid diluents. *J Polym Sci B Polym Phys* 32:523–533. <https://doi.org/10.1002/polb.1994.090320313>
- [52] Tábi T, Sajó IE, Szabó F, Luyt AS, Kovács JG (2010) Crystalline structure of annealed polylactic acid and its relation to processing. *EXPRESS Polym Lett* 4:659–668. <https://doi.org/10.3144/expresspolymlett.2010.80>
- [53] Nofar M, Tabatabaei A, Ameli A, Park CB (2013) Comparison of melting and crystallization behaviors of polylactide under high-pressure CO<sub>2</sub>, N<sub>2</sub>, and He. *Polymer* 54:6471–6478. <https://doi.org/10.1016/j.polymer.2013.09.044>
- [54] Yin G, Zhao D, Zhang L, Ren Y, Ji S, Tang H, Zhou Z, Li Q (2016) Highly porous 3D PLLA materials composed of nanosheets, fibrous nanosheets, or nanofibrous networks: preparation and the potential application in oil–water separation. *Chem Eng J* 302:1–11. <https://doi.org/10.1016/j.cej.2016.05.023>
- [55] Chang CJ, Day C-Y, Ko C-M, Chiu K-L (1997) Densities and P-x-y diagrams for carbon dioxide dissolution in methanol, ethanol, and acetone mixtures. *Fluid Ph Equilibria* 131:243–258. [https://doi.org/10.1016/S0378-3812\(96\)03208-6](https://doi.org/10.1016/S0378-3812(96)03208-6)
- [56] Galicia-Luna LA, Ortega-Rodriguez A, Richon D (2000) New apparatus for the fast determination of high-pressure vapor–liquid equilibria of mixtures and of accurate critical pressures. *J Chem Eng Data* 45:265–271. <https://doi.org/10.1021/jc990187d>
- [57] Mehl A, Nascimento FP, Falcão PW, Pessoa FLP, Cardozo-Filho L (2011) Vapor-liquid equilibrium of carbon dioxide + ethanol: experimental measurements with acoustic method and thermodynamic modeling. *J Thermodyn* 2011:1–11. <https://doi.org/10.1155/2011/251075>

**Publisher's Note** Springer Nature remains neutral with regard to jurisdictional claims in published maps and institutional affiliations.